Journal of Molecular Imaging & Dynamics

ISSN: 2155-9937

Gálisová et al., J Mol Imag Dynamic 2016, 6:1
DOI: 10.4172/2155-9937.1000121

Research Article Open Access

Magnetic Resonance Visualization of Pancreatic Islets Labeled by PARACEST Contrast Agents at 4.7 T

Andrea Gálisová[1], Daniel Jirák[1,2]*, Tereza Krchová[3], Vít Herynek[1], Eva Fábryová[4], Jan Kotek[3] and Milan Hájek[1]

[1]*MR Unit, Department of Radiodiagnostic and Interventional Radiology, Institute for Clinical and Experimental Medicine, Prague, Czech Republic*
[2]*Institute of Biophysics and Informatics, 1st Medicine Faculty, Charles University, Prague, Czech Republic*
[3]*Department of Inorganic Chemistry, Faculty of Science, Charles University, Prague, Czech Republic*
[4]*Center of Experimental Medicine, Institute for Clinical and Experimental Medicine, Prague, Czech Republic*

Abstract

Introduction: Monitoring of Pancreatic Islets (PIs) after their transplantation could provide important data related to diabetes treatment; however their visualization is conditioned by the contrast agent use. The aim of this study was to label and visualize PIs labeled by the contrast agents based on Chemical Exchange Saturation Transfer (CEST) owing an advantage of contrast switching on/off and simultaneous visualization of differently treated cell populations in one MR experiment.

Material and methods: Two paramagnetic chelates with europium Eu-DO3A-ae and ytterbium Yb-DO3A-ae were tested for labeling of PIs by pinocytosis and microporation. The toxicity, labeling efficacy and detection threshold were assessed for each agent. *In vitro* MR imaging of the labeled islets was performed on a 4.7 T scanner using a modified turbo spin-echo (RARE) sequence.

Results: The sufficient labeling efficacy was observed only by using high agent concentration compromising islet viability. The microporation procedure was not effective for islet labeling because of its invasive nature. The islets labeled by pinocytosis were visualized in a phantom by CEST imaging, however, after a long acquisition time at 4.7 T.

Conclusion: The low sensitivity of detection and impaired cellular viability of the pancreatic islets labeled by the novel CEST contrast agents represent a challenge for the further implementation of these probes as exogenous cellular labels.

Keywords: Pancreatic islets; Contrast agents; Magnetic resonance imaging; Chemical exchange saturation transfer; PARACEST

Introduction

Visualization and long-term tracking of transplanted pancreatic islets by Magnetic Resonance Imaging (MRI) is a well-established method and it has been successfully implemented also in the clinical practice [1,2]. Transplantation of Pancreatic Islets (PI) ensures regulation of the blood glucose level in instable type 1 Diabetes Mellitus (DM1) patients [3], however only around 20% of islet recipients at 5 years post-engraftment reached insulin independence [4]. Various factors contribute to immediate or long-term graft loss and function impairment [5], therefore a reliable method, which would elucidate the processes underlying islet engraftment and rejection in correlation with graft function, size and localization, is needed [6]. For accurate and specific monitoring of transplanted pancreatic islets, MRI seems to be a tool of choice because of its non-invasiveness, high spatio-temporal resolution and the possibility of highlighting the transplanted cells by suitable contrast agents.

Monitoring of the distribution and fate of transplanted islets by *in vivo* MRI was for the first time carried out in a rodent model of intrahepatic islet transplantation [7]. In this study, the islets were labeled *in vitro* by Superparamagnetic Iron Oxide Nanoparticles (SPION), which alter MRI signal intensity by enhancing the relaxation processes. Furthermore, the use of T_2/T_2^* contrast agents was implemented in the prediction of graft rejection [8,9] and it was integrated also in a clinical practice in DM1 patients [1,2]. The sensitivity of iron-oxide nanoparticles detection is very high and it is possible to visualize not only a single SPION-labeled islet [7] but even a single SPION-labeled macrophage cell *in vivo* in a mouse model [10]. Despite adequate properties of T_2/T_2^* contrast agents, a strong effect on magnetization beyond the actual size of the islets does not enable absolute quantification. In addition, the quantification is challenging because of negative contrast arising from the local inhomogeneities in the tissue. Another islet labeling approach is the use of T_1 contrast agents based on the lanthanide chelates which generate preferable hyperintense signal on the T_1-weighted MR images. *In vivo* visualization of Gd-HPDO3A-labeled islets has been already reported [11]; however these agents exploit lower imaging sensitivity requiring high agent uptake or high number of the cells. It was estimated that the minimum detectable number of Gd-HPDO3A-labeled cells is approximately 10^3 *in vitro* [12]. Another possibility to visualize pancreatic islets is utilization of non-proton MRI with suitable labels as fluorine ^{19}F-based agents [13]. Such a label possesses high specificity due to negligible natural fluorine abundance in the tissue but with the drawback of low detection sensitivity compared to ^{1}H MRI.

An indirect approach to detect pancreatic islets or beta cell mass might be the use of MR contrast agents responsive to concentration of metal ions which are specific for beta cell function and which

***Corresponding author:** Daniel Jirák, MR Unit, Department of Radiodiagnostic and Interventional Radiology, Institute for Clinical and Experimental Medicine, Prague, Czech Republic, Tel: +420 26136 2702; E-mail: daniel.jirak@ikem.cz

Received November 25, 2015; **Accepted** January 14, 2016; **Published** January 16, 2016

Citation: Gálisová A, Jirák D, Krchová T, Herynek V, Fábryová E, et al. (2016) Magnetic Resonance Visualization of Pancreatic Islets Labeled by PARACEST Contrast Agents at 4.7 T. J Mol Imag Dynamic 6: 121. doi:10.4172/2155-9937.1000121

can shorten T_1 relaxation times. The changes of beta cell mass were observed by detection of Mn^{2+} which enters the beta cell through the voltage-gated calcium channels upon glucose stimulation [14] or Zn^{2+} which is co-released with insulin and can be detected without glucose stimulation [15].

The relatively new MR contrast agents based on chemical exchange saturation transfer (CEST) [16] might bring other possibilities in cellular imaging. CEST principle is based on frequency selective saturation of exchangeable non-bulk water protons in the solute and subsequent exchange between the solvent and solute pools, which enables indirect observation of the low concentrated solute pool. The main advantage of CEST imaging is the possibility selectively switch the contrast on/off and visualize more than one agent in the same MR experiment [17]. CEST-MRI plays an important role in molecular imaging allowing detection of various endogenous metabolites [18-21] and estimation of additional microenvironmental and physiological parameters such as temperature and pH [22,23] or enzyme [24] and redox activity [25]. Moreover, strongly shifted paramagnetic compounds (PARACEST) were already applied in cellular labeling and visualization; europium/ytterbium-labeled tumor cells and macrophages were differentiated in one experiment [17,26]. Recently, the simultaneous visualization of neural stem cells and endothelial cells in a model of stroke has been reported [27]. Despite the reported visualization of the transplanted cells by PARACEST approach, the authors discussed the low detection sensibility and intracellular reduction of the CEST effect [27].

Because of the promising properties of CEST probes, we hypothesized that labeling of pancreatic islets by the CEST agents might help to specifically localize and monitor distribution of transplanted islets in the tissue. The implementation of the CEST approach for differentiation of the islets of different size or treated by the different drugs could bring an additional value into the post-transplant monitoring of the islet engraftment. In this study, we aimed to label and visualize pancreatic islets by two recently introduced PARACEST compounds [28] based on the DO3A chelates with exchangeable amino groups causing the CEST effect at various frequency offsets allowing their selective visualization. Various labeling approaches, such as pinocytosis or microporation, could be implemented for probe internalization inside the cell. Microporation as a type of electroporation uses a pipette tip as an electroporation space and higher voltage compared to conventional electroporation in a cuvette. The main advantage of microporation is probe incorporation in the cytoplasm because the agent stays entrapped in the endosomal vesicles after pinocytosis. The additional endosomal membrane can lead to lower saturation transfer effect due to limited accessibility of the cytosol water molecules as their free diffusion is blocked by membrane structures [17,29]. Moreover, the endosomal pH is lower than in cytoplasm and some CEST agents (including the tested ones, [28]) are pH sensitive and CEST signal may decrease at low pH values. The main goal of the study was to assess the labeling efficiency of two CEST probes using two labeling approaches to achieve high uptake of the agents for sufficient detection of labeled pancreatic islets at a 4.7 T scanner.

Material and Methods

Preparation and characterization of PARACEST contrast agents

Two paramagnetic lanthanide(III) complexes of H_3DO3A-ae with a different central-bound metal ion europium (Eu-DO3A-ae) or ytterbium (Yb-DO3A-ae) were synthesized as described previously [28]. Briefly, the ligand H_3DO3A-ae was prepared by reaction of t-Bu_3DO3A by alkylation with N-(2-bromoethyl)-phthalimide followed by sequential deprotection by trifluoroacetic acid and hydrazine. The ligand H_3DO3A-ae was purified by chromatography on an anion exchanger and by crystallization from hot EtOH with 59% overall yield. The Ln(III) complexes of H_3DO3A-ae were prepared by mixing the ligand with 1.1 equiv. of corresponding Ln(III) chloride in small amount of distilled water and adjusting pH of the mixture to ~6 with 1 M aq. NaOH. The mixture was stirred overnight at 60°C. Then the pH was re-adjusted to 6.5 and the solution was again stirred overnight at 60°C. The complex was purified on Al_2O_3 column by chromatography. The pure product [Ln(DO3A-ae)] was eluted using a mixture of EtOH:H_2O:conc. aq. NH_3 (10:8:1). The chemical structure of the final complexes is shown in Figure 1A.

The relaxation times of the 40 mM solutions of the compounds were measured on a 4.7 T scanner (Bruker BioSpin, Germany) at 25°C. T_1 relaxation time was calculated from a series of the images acquired by a spin echo sequence with variable repetition time (TR=6400 ms, 3200 ms, 1600 ms, 800 ms, 400 ms, 200 ms, 100 ms, 50 ms) and time to echo (TE=7.2 ms) and acquisition time 5 min per one image. T_2 relaxation time was measured by a CPMG (Carl Purcell Meiboom Gill) sequence with following parameters TR=5000 ms, TE=7.2 ms 256 echoes, total acquisition time 21 min. T_1 and T_2 relaxation times were calculated by performing a mono-exponential fit of the mean pixel intensity of a selected region at the different sampling time by using the software GraphPad Prism (GraphPad Software Inc, San Diego, CA).

Isolation and labeling of pancreatic islets

Pancreatic islets were isolated from Brown-Norway rats (n=12) according to a standard protocol [30] and following the institutional and national guidelines for the care and use of animals. Briefly, the pancreas was digested by the slow injection of collagenase solution (1mg/mL, 15 mL for a rat; Sigma Aldrich, USA) into the pancreatic duct. The pancreas was then carefully excised and shaken at 37°C for 20 min. Islets were separated from the exocrine tissue using centrifugation in discontinuous Ficoll gradient (1.037, 1.069, 1.096, 1.108 g/mL; Sigma Aldrich, USA). The isolated islets were then incubated (37°C, 5% CO_2 atmosphere) in CMRL-1066 culture medium supplemented with 1% HEPES buffer, 10% fetal bovine serum and 1% penicillin/streptomycin/L/glutamine (Sigma Aldrich, USA). After overnight incubation, the islets were labeled either by pinocytosis or microporation.

Labeling by pinocytosis was accomplished by incubation of the islets in the culture medium with different concentrations of the CEST

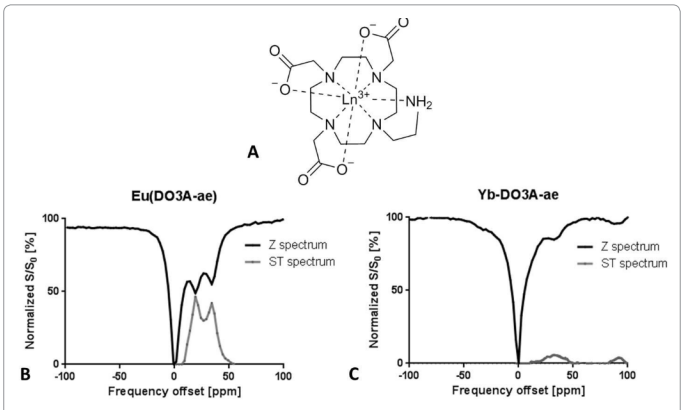

Figure 1: Formula of the H_3DO3A-ae chelates used as the CEST contrast agents in this study (A). Z-spectra of the 50 mM aqueous solution of Eu-DO3A-ae (B) and Yb-DO3A-ae (C) measured at 4.7 T.

agents (30, 45, 60, 80, 100 mM) for 12 or 24 hours. Microporation was performed using a Neon™ transfection system (Invitrogen, CA, USA). Prior the procedure, about 300 islets were mixed with resuspension buffer containing 60 or 100 mM of Eu/Yb-DO3A-ae. The islets were then electroporated in the microporation capillary with two 20 or 30 ms pulses of various voltages (600, 800, 1000 V). After microporation, the islets were kept on ice for 10 min and then incubated overnight in the culture medium without antibiotics at 37°C. The control sample contained the islets incubated in the medium without the contrast agents. After labeling, the islets were washed three times with PBS. For the MRI experiment, the islets were placed into the tube with PBS or into a phantom between two gelatin layers (3% upper layer and 4% lower layer to prevent the islets to fall to the bottom). During the microporation procedure, only a part of the islets survived, therefore approximately 50-150 islets were transferred into the phantom. The exact number of islets in the phantom is listed in the corresponding figure legend. For *in vitro* MRI of pancreatic islets, the most promising labeling conditions regarding islet viability and agent uptake were used: pinocytosis 60, 80, 100 mM for 24 hours; microporation with 100 mM concentration of the agents with two 20 ms or 30 ms pulses and voltage of 800 V. The microporated islets were placed into the gelatin phantom. The control samples contained the islets incubated in the medium without contrast agents (100 islets for ICP-MS examination, 100 islets for evaluation of the stimulation index). The controls were then processed and evaluated in the same way as the samples containing labeled islets.

Viability assays and functional tests

Islet viability was evaluated under the fluorescent microscope after staining with Propidium Iodide and Acridine Orange (Sigma Aldrich, USA). The ratio of the viable cells to all cells inside the islets was assessed for 10 randomly chosen islets and expressed as an average percentage. The capability to produce insulin was measured by static incubation of the islets in the media with low (3.3 mM) and high (22 mM) glucose concentrations and expressed as a stimulation index for each concentration. The stimulation index was calculated as a ratio of the insulin values measured from the high and low glucose samples.

ICP-QMS measurements

The uptake of the complexes into the islets was determined by inductively coupled plasma quadrupole mass spectrometry (ICP-QMS). After washing with PBS three times, the labeled islets were digested using 250 µL of concentrated HNO_3 and dried in a desiccator (NaOH) equipped with a drying tube ($CaCl_2$) for 24 hours at 90°C. The drying process was repeated twice; then each sample was dissolved in 5 or 10 mL of 2% (v/v) HNO_3. The blank sample contained only 2% (v/v) HNO_3. ICP-QMS analysis was performed using a Thermo Scientific X Series II quadrupole ICP mass spectrometer on the commercial basis at the Faculty of Science, Charles University in Prague, Czech Republic. The standard deviations were calculated from two measurements of the same sample. The uptake of the agents was estimated as a number of complexes incorporated in one islet or cell. For assessment of the feasibility of labeled islet visualization, an approximate concentration of the agents in a suspension containing 1000 islets per 50 µL was calculated.

CEST MR experiments and data analysis

MR imaging was carried out on the 4.7 T MR scanner using a resonator coil with a diameter of 7 cm (Bruker BioSpin, Germany).

The parameters for CEST imaging were optimized in a separate experiment. The Z-spectra from 50 mM concentration of the agents were obtained by acquisition of a series of images using a RARE sequence with the major parameters: TR/TE=5000 ms/8.9 ms, RARE factor=16, matrix size of 128 × 128, the field of view (FOV)=55 × 55 mm, 2 dummy scans and slice thickness of 2 mm. The readout was preceded by a 3000 ms long pre-saturation Gaussian pulse at a power level of 35 µT with variable frequency offsets ranging from +100 ppm to -100 ppm with the step of 2.5 ppm (81 images).

Phantoms containing 1.25–40 mM of both PARACEST agents dissolved in water were prepared in the glass tubes and immersed in 4% gelatin (Figure 2A and 2B). For CEST acquisition of the phantoms, the same MR parameters were used as for the acquisition of the Z-spectra. Contrast-To-Noise Ratios (CNR) were calculated for each concentration according to a formula

$$CNR = \frac{I(-) - I(+)}{\sqrt{\sigma^2(-) + \sigma^2(+)}} \quad (1)$$

where σ^2 represents standard deviations of the noise region.

The theoretical threshold $CNR_{threshold}$ for *in vivo* visualization according to Liu [31] is

$$CNR_{threshold} = 2\sqrt{2}. \quad (2)$$

CNR values were experimentally assessed for various agent concentrations of both CEST (Figure 2J) and the lowest detectable concentration, which produces CNR higher than the theoretical threshold was determined.

The islets labeled by 60 mM, 80 mM and 100 mM concentration were examined by *in vitro* CEST imaging. The parameters for *in vitro* CEST imaging were similar as for the phantom study with the solutions; only the slice thickness was lower due to the small islet layer in the phantom and two image resolutions were tested (128 × 128 and 256 × 256). In the case of failure of islet detection using within 3.5 or 20 min per one frequency offset, the acquisition time was prolonged to 1 hour. The exact parameters and the numbers of the examined islets are listed in the figure captions.

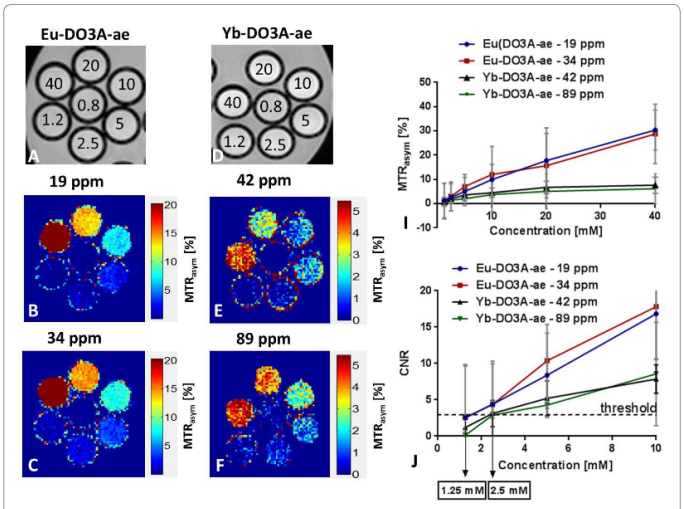

Figure 2: MR characterization of the contrast agents. The reference MR reference images (A, B) of the phantom containing various concentrations of Eu-DO3A-ae (B, C) and Yb-DO3A-ae (E, F) compounds. The numbers represent milimolar concentration of the agents. MTR_{asym} maps obtained after saturation at the frequency offset 19 ppm and 34 ppm for Eu-DO3A-ae and at 42 ppm and 89 ppm for Yb-DO3A-ae. Dependence of the MTR_{asym} values (I) and contrast-to-noise ratios (CNR) (J) on the agent concentration. The dotted line represents the detection CNR*threshold* and the minimal detectable concentration which can reach CNR above this threshold is depicted in the square.

The CEST effect was expressed an assymetric magnetic transfer ratio (MTR_{asym}) and calculated from a chosen region of interest on the pixel wise basis using a definition

$$MTR_{asym} = \frac{I(+) - I(-)}{I(-)} \times 100\% \quad (3)$$

where I(+) and I(−) are the signal intensities acquired after saturation at the positive or negative frequency offsets, respectively. MTR_{asym} maps were reconstructed after noise thresholding and expressed in a false-color scale in percentage units using a custom written script in Matlab (Mathworks, Natick, MA, USA).

Statistical analysis

The statistical analysis was performed by using the GraphPad Prism (GraphPad Software Inc, San Diego, CA). The mean values and standard deviations are presented in the graphs.

Results

Characteristics of the PARACEST agents

The CEST NMR experiment revealed water saturation after irradiation of Eu-DO3A-ae and Yb-DO3A-ae complexes at specific frequencies as a result of slow exchange of exchangeable protons between the amino groups of the complexes and bulk water. The Z-spectra of Eu-DO3A-ae (Figure 1B) and Yb-DO3A-ae (Figure 1C) show a dependence of the normalized water signal intensity on the frequency offsets assessed as the chemical shifts to the signal of the bulk water protons (0 ppm). The saturation maxima were found at 19 ppm and 34 ppm for Eu-DO3A-ae and at 42 ppm and 89 ppm for Yb-DO3A-ae. Two peaks arose from two amine hydrogen atoms, which became non-equivalent after group coordination [28]. The observed CEST signals in the Z-spectra of 50 mM Eu-DO3A-ae had higher CEST effect (47% and 43% MTR_{asym}) compared to 50 mM Yb-DO3A-ae (8% and 4% MTR_{asym}). The peaks of Eu-DO3A-ae overlapped with the peak of Yb-DO3A-ae at 42 ppm. The relaxation times of Eu-DO3A-ae (T_1=1436 ± 24 ms, T_2=480 ± 47 ms) were higher than for Yb-DO3A-ae (T_1=599 ± 17 ms, T_2=331 ± 39 ms).

The MTR_{asym} maps of the phantoms containing the agents of various concentration showed proportional signal intensity dependence upon agent concentration (Figure 2B-2I). Calculation of CNR revealed that the minimal detectable concentration for MRI imaging (detection threshold) was 1.25 mM for Eu-DO3A-ae and 2.5 mM for Yb-DO3A-ae (Figure 2J).

Labeling of islets by CEST agents

In vitro labeling of pancreatic islets was accomplished by two methods-pinocytosis and microporation. ICP-QMS analysis showed that pinocytosis led to incorporation of approximately 8.3×10^{12}-2.9×10^{14} complexes per one islet (i.e., 4.2×10^{9}-1.5×10^{11} per cell) what represents maximum concentration up to 10 mM. For cell labeling, simple pinocytosis was found to provide slightly better results compared to microporation. Using microporation, maximum of 1.3×10^{13}-2.3×10^{13} (i.e., 6.5×10^{9}- 1.1×10^{10} per cell) of complexes were loaded into one islet what was lower amount compared to pinocytosis with 30 mM concentration of the CEST agents in the medium for 24 hours. The use of microporation led to destruction of approximately 70% of islets and the islet viability decreased. Dead cells in the microporated islets were localized mostly in the islet center (Figure 3A) in comparison to pinocytosis; in this case the dead cells were detected at the islet surface (Figure 3A). The use of a higher concentration of the CEST probes in the incubation medium led to higher uptake of both complexes (Figure 4A and 4B). Similarly, incubation of the islets for a longer time led to higher agent internalization into the cells (Figure 4A and 4B). The highest uptake of both agents was observed after incubation in the medium with 80 mM agent concentration (Figure 4A and 4B). However, lower concentration (30, 45, 60 mM of Eu-DO3A-ae and 45 mM of Yb-DO3A-ae) (Figure 4A and 4B) also reached the border of the detection threshold. Microporation did not reach the detection threshold (Figure 4C). It is important to note that high concentration for pinocytosis affected islet viability, which decreased below 70% at concentrations higher than 60 mM during 24 hour incubation. Moreover, estimation of the stimulation indexes of the labeled islets revealed that the agent concentration above 60 mM significantly impaired insulin secretion and islet function. The data are summarized in the Table 1.

Visualization of pancreatic islets labeled by CEST agents

In the MR experiment, no CEST signal from the islets labeled with 60 mM concentration of Eu-DO3A-ae and Yb-DO3A-ae was detected within 7 minutes of acquisition after saturation at the specific frequency offsets (Figure 5B-5E). Similarly, no CEST effect was observed from the islets labeled by higher concentration (100 mM) within 40 minutes of acquisition (Figure 6B and 6C). For detection, the acquisition time had to be prolonged up to 1-2 hours. In this case, approximately 300 islets labeled with 100 mM of Eu-DO3A-ae complex in a gelatin phantom were visualized with 20% MTR_{asym} value (Figure 6E). 200 islets labeled with 80 mM of Eu-DO3A-ae were also detected and reached around 8% MTR_{asym} (Figure 6H). The islets labeled by 100 mM concentration of Yb-DO3A-ae reached only 3% MTR_{asym} (Figure 6F) and the islets labeled by 80 mM of Yb-DO3A-ae had no CEST signal even after 2 hours of acquisition time (Figure 6I).

The islets microporated with 100 mM of the CEST agents were not detected by CEST imaging (Figure 6E, 6F, 6H and 6I). In this case only a small number of islets survived the microporation procedure and approximately 15-50% of the original islet number was transferred into the gelatin phantom.

The islets labeled by Eu-DO3A-ae showed low MTR_{asym} values (4%) after Yb-specific irradiation at 89 ppm (Figure 6F and 6I) and similarly the islets labeled Yb-DO3A-ae provided also some CEST effect (10-15%) after Eu-specific irradiation at 34 ppm (Figure 6E and 6H).

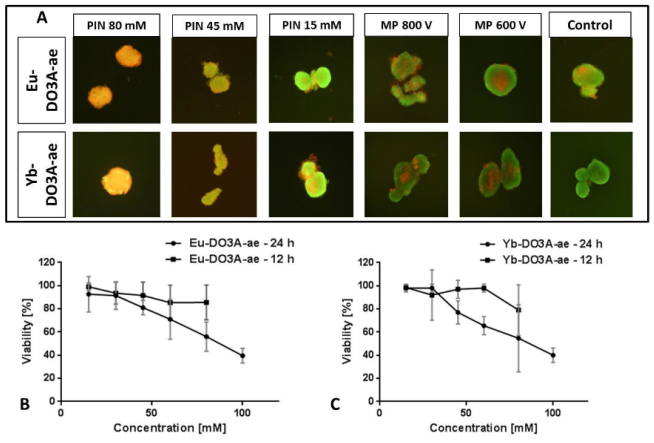

Figure 3: Comparison of islet viability after 24 hours labeling by pinocytosis (PIN), after microporation (MP) and the control islets (A). The fluorescent images represent color-coded viability, red color for dead cells and green color for viable cells. The plots show islet viability after labeling by Eu-DO3A-ae (B) and Yb-DO3A-ae (C) compounds expressed as a percentage of the viable cells.

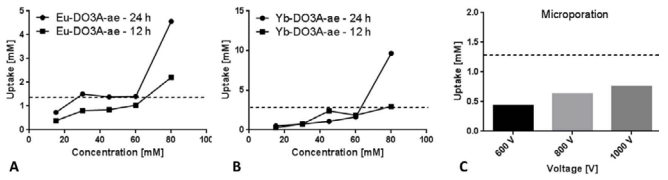

Figure 4: Uptake of the complexes into the islets after labeling by pinocytosis using different concentration of Eu-DO3A-ae (A) and Yb-DO3A-ae (B) and by microporation using different voltage (600 V, 800 V, 1000 V) (C). The standard deviations are below 1%. The dotted lines stands for the detection threshold calculated from CNR of the pure agents.

PARACEST complex	Concentration [mM]	Viability after 24 h Incubation [%]	Viability after 12 h Incubation [%]	Stimulation index
Eu-DO3A-ae	100	40.0 ± 6.43	NA	NA
	80	56.0 ± 12.65	85.6 ± 15.05	0.60 ± 0.18
	60	71.0 ± 17.13	85.3 ± 13.15	2.11 ± 1.28
	45	81.0 ± 6.15	91.5 ± 11.56	2.05 ± 1.56
	30	91.4 ± 11.97	92.5 ± 9.44	NA
	15	92.7 ± 15.39	99.0 ± 3.16	NA
Yb-DO3A-ae	100	39.5 ± 6.23	NA	NA
	80	54.2 ± 9.04	79.0 ± 21.83	0.94 ± 0.11
	60	65.5 ± 7.89	98.0 ± 3.49	1.98 ± 1.79
	45	77.0 ± 10.05	97.1 ± 7.75	1.24 ± 0.20
	30	98.0 ± 3.49	92.0 ± 12.88	NA
	15	98.0 ± 3.02	98.5 ± 2.42	NA
Control	0	98.0 ± 3.49	98.5 ± 2.41	2.14 ± 1.47

Table 1: Data summary from assessment of viability and stimulation index corresponding to insulin production of the pancreatic islets labeled by pinocytosis. NA – data not assessed.

Discussion

CEST agents represent a new class of MRI contrast agents [16] with advantages over the conventional superparamagnetic and paramagnetic cellular probes. The paramagnetic agents based on DO3A chelates examined in this study could serve as exogenous PARACEST contrast agents due to a slow exchange between the protons of their amino groups and bulk water [28]. Moreover, the tested PARACEST probes exploit similar chemical structure as clinically approved MRI contrast agents (e.g. Gd-HPDO3A) and due to the large chemical shift of the resonance frequency of the exchangeable protons from the water frequency, direct water saturation is minimized which is preferable for *in vivo* measurements. Because of the suitable properties of our probes for CEST imaging, we tested the feasibility of Eu-DO3A-ae and Yb-DO3A-ae complexes for visualization of pancreatic islets intended for cell therapy of diabetes.

The europium-based analogue displayed higher CEST effect compared to ytterbium complex. The lower relaxation time of Yb-DO3A-ae could also contribute to its lower CEST signal. Similarly, the calculation of the detection threshold demonstrated better sensitivity of Eu-DO3A-ae than Yb-DO3A-ae. Our results indicate that the uptake of the imaging probes should be higher than 1.25 mM for Eu-DO3A-ae-labeled cells and more than 2.5 mM for Yb-DO3A-ae-labeled cells for the sufficient visualization. To assess the most efficient islet labeling, two labeling routes-pinocytosis and microporation were compared and the internalization of the agents and functional status of the labeled PIs were assessed. In general, microporation could lead to higher CEST detection due to higher pH in cytoplasm and no quenching by additional endosomal membrane as it occured by pinocytosis [29].

In our study, only one labeling condition led to the agent uptake above the detection threshold: pinocytosis with minimal concentration of 80 mM of both agents. Unfortunately, higher concentration caused substantial decrease of PI viability suggesting a harmful effect of the probes to the cells. In addition, the insulin secretion of the labeled islets was impaired using higher concentrations of the complexes. Acceptable islet function and viability was obtained after pinocytosis with less than 60 mM concentration in the incubation medium only. This condition would reach just the border of detection threshold for sufficient visualization of 1000 islets at 4.7 T magnetic field. Although increasing uptake with increasing concentration is expectable; the prominent difference between 60 and 80 mM may be related to substantial damage to the islets. We speculate that high uptake may be caused by higher entrapment of the complexes in the extracellular space of the islets due to higher impairment.

The difference in the cell viability after labeling during 12 and 24 hours could be explained by the longer exposure of islets to the contrast agent. If the agent is entrapped into the endosomes, the lanthanide ion could be released and affect the cell viability. By prolongation of the incubation time, more complexes are entrapped inside the cells and therefore the viability is decreased. Experience with the labeling of pancreatic islets by iron oxide nanoparticles showed that the contrast agent is located initially at the periphery and later also inside the islets [32]. We hypothesize that the similar effect may occur also with this type of small molecules.

Labeling of PIs using microporation was not proven to be optimal and it did not reach the detection threshold in our study. High-voltage microporation is an invasive method and a lot of islets were destroyed during the microporation procedure, although the function of the survived islets was not markedly impaired. Up to now, microporation was mostly used to transfect the various types of cells [33] and based on our results it seems not to be an optimal method for pancreatic islets labeling.

MRI experiment proved than *in vitro* visualization of PIs labeled by Eu-DO3A-ae agent is possible; however long acquisition time is unacceptable for *in vivo* experiments. The labeled islets were detected

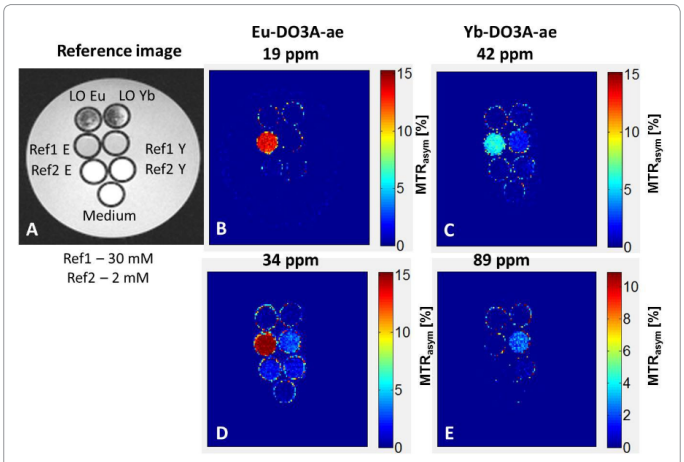

Figure 5: *In vitro* CEST MRI visualization of the pancreatic islets in PBS. MTR_{asym} maps of 1000 labeled islets obtained by saturation at various frequency offsets: 19 ppm (B), 34 ppm (C), 42 ppmz (D) and 89 ppm (E). The islets were labeled by pinocytosis using 60 mM concentration of the complexes. The control samples contain the solutions of the agents or incubation medium. The MR parameters: RARE sequence, TR/TE = 5000 ms/8.9 ms, matrix size 128x128, slice thickness 1.5 mm. Measurement time per one frequency offset was 3.5 minute.

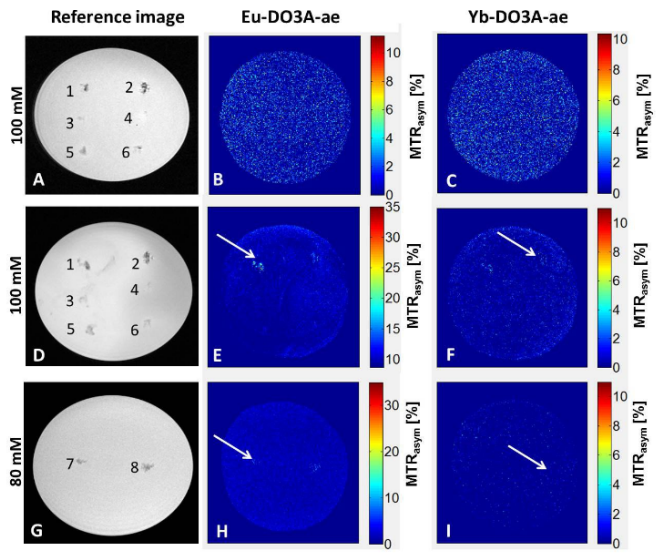

Figure 6: *In vitro* CEST MRI visualization of the labeled pancreatic islets in a gelatin phantom. A reference MR image of a gelatin phantom containing the labeled pancreatic islets **(A, D, G)**. MTR_{asym} maps of the phantom with saturation at 34 ppm for Eu-DO3A-ae **(B, E, H)** and with saturation at 89 ppm for Yb-DO3A-ae **(C, F, I)**. The labeling conditions for each group: (1) pinocytosis Eu-DO3A-ae, 300 PI; (2) pinocytosis Yb-DO3A-ae, 380 PI; (3) microporation Eu-DO3A-ae 800V for 20 ms, 60 PI; (4) microporation Yb-DO3A-ae 800V for 20 ms, 60 PI; (5) microporation Eu-DO3A-ae 800V for 30 ms, 150 PI; (6) microporation Yb-DO3A-ae 800V for 30 ms, 170 PI; (7) pinocytosis Eu-DO3A-ae, 200 PI; (8) pinocytosis Yb-DO3A-ae, 200 PI. The MR parameters: RARE sequence, TR/TE = 5000 ms/8.9 ms, matrix size 256x256, slice thickness 1 mm Measurement time per one frequency offset: B, C – 20 min; E, F – 1 hour. The arrow points the islets which should be visualized at the chosen frequency offset.

after 1 hour of data acquisition and only the islets labeled by high concentration of the agents (80 or 100 mM) compromising islets viability were visible. In another study, the macrophages and murine melanoma cells were successfully labeled by Eu- and Yb-HPDO3A complex without viability loss using 100 mM concentration of the contrast agents [17]. The same authors published another paper about the loading of Dy-HPDO3A inside the red blood cells for the shifting of intracellular water [34]. In contrast to our experiments at 4.7 T, both studies held by this group were performed at 7 T magnetic field using a microimaging probe. In the recent study, neural stem cells and endothelial cells labeled by Yb-/Eu-HPDO3A were visualized *in vivo* in a model of stroke at 9.4 T [27]. These results indicate that higher magnetic fields than 4.7 T might be favorable due to higher MR signal, longer T_1 relaxation times and higher frequency distance between amine and water protons.

A weak signal from the Yb-DO3A-ae labeled PIs even during Eu-specific was caused by overlapping of the peaks of both compounds in the Z-spectra (Figure 6F and 6I). Low MTR_{asym} value of the islets labeled by Eu-DO3A-ae after Yb-specific irradiation could correspond to the statistical error (Figure 6E and 6H).

Low CEST signal detection in our study could be explained by low sensitivity of the tested CEST agents at 4.7 T and by pH-sensitive decrease of CEST effect in the endosomes after labeling by pinocytosis. The decreasing CEST signal of the agents at lower pH was already reported [28]. The endosomes have lower pH than cytoplasm and after fusion with lysosomes, pH becomes even more acidic. Acidity might therefore directly affect the CEST signal from the labeled islets in our study. Moreover, this effect probably contributed to the toxicity of the agents because the metal ion could be slowly released from the ligand at acidic pH (pH<6) and compromise the islet viability [28].

Additionally, the assessment of the CEST effect is very sensitive to B_0/B_1 field inhomogeneities [35,36]. The magnetic field inhomogeneities arising from the inter-voxel physical differences may affect the accuracy of determination of the CEST effect [37] and this effect could be prominent especially in the case of cellular imaging where high resolution is demanding. We tested also an evaluation protocol with B_0 correction including acquisition of the full range of Z-spectrum and zero-offset correction so-called WASSR approach [36] with only negligible sensitivity improvement and substantial prolongation of the acquisition time. Also, the choice of imaging pulse sequence and saturation pulses could play a role in the CEST imaging [35], however, the biggest limitation represents a saturation pulse (we used a long and strong Gaussian pulse), which might easily exceed SAR restrictions in *in vivo* setting.

Despite the described obstacles, exogenous CEST agents with improved properties represent a potential tool for future clinical applications. A recent study showed the dependence of transplantation outcome on the islet size with superior properties of the smaller islets [38]. Be labeling of the islets by various CEST agents, their visualization and discrimination according to their size could be performed noninvasively *in vivo* and the transplantation outcome could be assessed. Also, discrimination of the islets treated by the different drugs and correlation with the therapy outcome could be performed during the treatment. Improvement of the agent properties regarding pH-dependent stability and toxicity could bring a hope in the future cellular labeling by these probes and their broader application.

Conclusion

The novel MR contrast agents based on the CEST effect were tested for labeling and visualization of pancreatic islets intended for type 1 diabetes mellitus treatment. The functional status of the labeled pancreatic islet was evaluated and *in vitro* MRI CEST imaging was carried out. Only high agent concentration for islet labeling reached a sufficient labeling efficacy for *in vitro* visualization, however low sensitivity at 4.7 T resulted in the extremely long acquisition time. Despite their potentiality, implementation of the novel CEST contrast agents as exogenous cellular labels requires further improvement of detection sensitivity and pH stability to minimize their toxicity.

Acknowledgements

The research leading to these results has received funding from the People Programme (Marie Curie Actions) of the European Union's Seventh Framework Programme FP7/2007-2013/ under REA grant agreement No. 289932, the Czech Science Foundation P207-11-1437 and by the MH CR-DRO (Institute for Clinical and Experimental Medicine IKEM, IN00023001").

Conflict of Interest

The authors declare that they have no conflict of interest.

References

1. Toso C, Vallee JP, Morel P, Frédéric Ris, Demuylder-Mischler S, et al. (2008) Clinical magnetic resonance imaging of pancreatic islet grafts after iron nanoparticle labeling. Am J Transplant 8: 701-706.
2. Saudek F, Jirák D, irman P, Herynek V, Dezortová M, et al. (2010) Magnetic Resonance Imaging of Pancreatic Islets Transplanted Into the Liver in Humans. Transplantation 90: 1602-1606.
3. Shapiro JAM, Lakey JRT, Edmond Ryan A, Gregory Korbutt S, Ellen Toth, et al. (2000) Islet transplantation in seven patients with type 1 diabetes mellitus using glucocorticoid-free immunosuppresive regimen. N Engl J Med 343: 230-238.
4. Low G, Hussein N, Owen RJ, Toso C, Patel VH, et al. (2010) Role of Imaging in Clinical Islet Transplantation. Radiographics 30: 353-366.

5. Barton FB, Rickels MR, Alejandro R, Hering BJ, Wease S, et al. (2012) Improvement in outcomes of clinical islet transplantation: 1999-2010. Diabetes Care 35: 1436-1445.

6. Arifin DR, Bulte JWM (2011) Imaging of Pancreatic Islet cells. Diabetes Metab Res Rev 27: 761-766.

7. Jirák D, Kříž J, Herynek V, Andersson B, Girman P, et al. (2004) MRI of transplanted pancreatic islets. Magn Reson Med 52: 1228-1233.

8. Jirák D, Kříž J, Strzelecki M, Yang J, Hasilo C, et al. (2009) Monitoring the survival of islet transplants by MRI using a novel technique for their automated detection and quantification. MAGMA 22: 257-265.

9. Kříž J, Jirák D, Berkova Z, Herynek V, Lodererova A, et al. (2012) Detection of pancreatic islet allograft impairment in advance of functional failure using magnetic resonance imaging. Transpl Int 25: 250-260.

10. Heyn C, Ronald J a, Mackenzie LT, MacDonald IC, Chambers AF, et al. (2006) In vivo magnetic resonance imaging of single cells in mouse brain with optical validation. Magn Reson Med 55: 23-29.

11. Biancone L, Crich SG, Cantaluppi V, Romanazzi GM, Russo S, et al. (2007) Magnetic resonance imaging of gadolinium-labeled pancreatic islets for experimental transplantation. NMR Biomed 20: 40-48.

12. Crich SG, Biancone L, Vincenzo Cantaluppi, Debora Duò, Giovanna Esposito, et al. (2004) Improved route for the visualization of stem cells labeled with a Gd-/Eu-chelate as dual (MRI and fluorescence) agent. Magn Reson Med 51: 938-944.

13. Barnett BP, Ruiz-Cabello J, Hota P, Ouwerkerk R, Shamblott MJ, et al. (2011) Use of perfluorocarbon nanoparticles for non-invasive multimodal cell tracking of human pancreatic islets. Contrast Media Mol Imaging 6: 251-259.

14. Antkowiak PF, Stevens BK, Nunemaker CS, McDuffie M, Epstein FH (2012) Manganese-Enhanced Magnetic Resonance Imaging Detects Declining Pancreatic Cell Mass in a Cyclophosphamide - Accelerated Mouse Model of Type 1 Diabetes. Diabetes 62: 44-48.

15. Lubag AJM, Leon-rodriguez LM De, Burgess SC, Sherry AD (2011) Noninvasive MRI of β -cell function using a Zn 2 + -responsive contrast agent. PNAS 108: 18400-18405.

16. Ward KM, Aletras AH, Balaban RS (2000) A new class of contrast agents for MRI based on proton chemical exchange dependent saturation transfer (CEST). J Magn Reson 143: 79-87.

17. Ferrauto G, Castelli DD, Terreno E, Aime S (2013) In vivo MRI visualization of different cell populations labeled with PARACEST agents. Magn Reson Med 69: 1703-1711.

18. Haris M, Cai K, Singh A, Hariharan H, Reddy R (2011) In vivo imaging of brain myo-inositol. Neuroimage 54: 2079-2085.

19. Haris M, Singh A, Kogan FS, Hariharan H, Reddy R, et al. (2012) Exchange rates of creatine kinase metabolites: feasibility of imaging creatine by chemical exchange saturation transfer MRI. NMR Biomed 25: 1305-1309.

20. Cai K, Haris M, Singh A, Kogan F, Greenberg JH, et al. (2012) Magnetic Resonance imaging of glutamate. Nat Med 18: 302-306.

21. Ren J, Trokowski R, Zhang S, Malloy CR, Sherry AD (2008) Imaging the tissue distribution of glucose in livers using a PARACEST sensor. Magn Reson Med 60: 1047-1055.

22. Delli Castelli D, Ferrauto G, Cutrin JC, Terreno E, Aime S (2014) In vivo maps of extracellular pH in murine melanoma by CEST-MRI. Magn Reson Med 71: 326-332.

23. McVicar N, Li AX, Suchý M, Hudson RH, Menon RS, et al. (2013) Simultaneous in vivo pH and temperature mapping using a PARACEST-MRI contrast agent. Magn Reson Med 70: 1016-1025.

24. Li Y, Sheth VR, Liu G, Pagel MD (2011) A self-calibrating PARACEST MRI contrast agent that detects esterase enzyme activity. Contrast Media Mol Imaging 6: 219-228.

25. Ratnakar SJ, Viswanathan S, Zoltan K, Ashish Jindal K, Kayla Greenet N, et al. (2012) Europium(III) DOTA-tetraamide complexes as redox-active MRI sensors. J Am Chem Soc 134: 5798-5800.

26. Aime S, Carrera C, Daniela DC, Simonetta GC, Enzo Terreno (2005) Tunable imaging of cells labeled with MRI-PARACEST agents. Angew Chem Int Ed Engl 44: 1813-1815.

27. Nicholls FJ, Ling W, Ferrauto G, Aime S, Modo M, et al. (2015) Simultaneous MR imaging for tissue engineering in a rat model of stroke. Sci Rep 5: 14597.

28. Krchová T, Kotek J, Jirák D, Havlíčková J, Císařová I, et al. (2013) Lanthanide(III) complexes of aminoethyl-DO3A as PARACEST contrast agents based on decoordination of the weakly bound amino group. Dalton Trans 42: 15735-15747.

29. Terreno E, Geninatti Crich S, Belfiore S, Biancone L, Cabella C, et al. (2006) Effect of the intracellular localization of a Gd-based imaging probe on the relaxation enhancement of water protons. Magn Reson Med 55: 491-497.

30. Kříž J, Jirák D, White D, Foster P (2008) Magnetic Resonance Imaging of Pancreatic Islets Transplanted Into the Right Liver Lobes of Diabetic Mice. Transplant Proc 40: 444-448.

31. Liu G, Ali MM, Yoo B, Griswold MA, Tkach JA, et al. (2009) PARACEST MRI with improved temporal resolution. Magn Reson Med 61: 399-408.

32. Berkova Z, Jirak D, Zacharovova K, Kriz J, Lodererova A, et al. (2008) Labeling of Pancreatic Islets With Iron Oxide Nanoparticles for In Vivo Detection With. Transplantation 85: 1550-1159.

33. Lim JY, Park SH, Jeong CH, Hyeon JO, Kim SM, et al. (2010) Microporation is a valuable transfection method for efficient gene delivery into human umbilical cord blood-derived mesenchymal stem cells. BMC Biotechnol 10: 38.

34. Ferrauto G, Delli Castelli D, Di Gregorio E, Langereis S, Burdinski D, et al. (2014) Lanthanide-loaded erythrocytes as highly sensitive chemical exchange saturation transfer MRI contrast agents. J Am Chem Soc 136: 638-641.

35. Liu G, Song X, Chan KWY, McMahon MT (2013) Nuts and bolts of chemical exchange saturation transfer MRI. NMR Biomed 26: 810-828.

36. Kim M, Gillen J, Landman BA, Zhou J, van Zijl PC (2009) WAter Saturation Shift Referencing (WASSR) for chemical exchange saturation transfer experiments. Magn Reson Med 61: 1441-1450.

37. Stancanello J, Terreno E, Castelli DD, Cabella C, Uggeri F, et al. (2008) Development and validation of a smoothing-splines-based correction method for improving the analysis of CEST-MR images. Contrast Media Mol Imaging 3: 136-149.

38. Zorzi D, Phan T, Sequi M, Lin Y, Freeman DH, et al. (2015) Impact of islet size on pancreatic islet transplantation and potential interventions to improve outcome. Cell Transplant 24: 11-23.